Laser-Induced Incandescence Study of Soot Formation in a Rapid Compression Machine at Elevated Pressures

Cyril Crua, David A. Kennaird, Morgan R. Heikal

Internal Combustion Engine Group, School of Engineering, University of Brighton, Brighton BN2 4GJ, UK

Published in: Combustion and Flame (http://www.elsevier.com/locate/combustflame)
Received 21 Dec 2002; received in revised form 02 Jun 2003; accepted 15 Jul 2003

Citation:
C. Crua, D.A. Kennaird, M.R. Heikal (2003) "Laser-induced incandescence study of diesel soot formation in a rapid compression machine at elevated pressures", Combustion and Flame, 135(4), 475-488.

Corresponding author:
Dr. Cyril Crua
Internal Combustion Engine Group
School of Engineering
Cockcroft Building
University of Brighton
Lewes Road
Brighton BN2 4GJ

Tel: +44 (0)1273 642 312
Fax: +44 (0)1273 642 444
E-mail: c.crua@brighton.ac.uk

Abstract

Simultaneous laser-induced incandescence (LII) and laser-induced scattering (LIS) were applied to investigate soot formation and distribution in a single cylinder rapid compression machine. The fuel used was a low sulphur reference diesel fuel with 0.04% volume 2-ethylhexyl nitrate. LII images were acquired at time intervals of 1 CA throughout the soot formation period, for a range of injection pressures up to 160 MPa, and in-cylinder pressures (ICP) up to 9 MPa. The data collected shows that although cycle-to-cycle variations in soot production were observed, the LII signal intensities converged to a constant value when sufficient cycles were averaged. The amount of soot produced was not significantly affected by changes in in-cylinder pressure. Soot was observed distributed in definite clusters, which were linked to slugs of fuel caused by oscillations in the injector needle. The highest injection pressure exhibited lower soot productions and more homogeneous soot distributions within the flame. Despite diffusion flames lasting longer with lower injection pressure, it appeared that the extended oxidation time was insufficient to oxidise the excess production of soot. In addition, soot particles were detected closer to the nozzle tip with higher injection pressures. The recording of LII sequences at high temporal resolutions has shown that three distinct phases in soot formation can be observed. First, high soot formation rates are observed before the establishment of the diffusion flame. Then, a reduced soot formation rate is apparent from the start of diffusion flame until the end of injection. Finally, high soot oxidation rates occur after the end of injection and for the duration of the flame.

1. Introduction

Diesel engine designers face increasingly severe regulatory limits on emissions from their engines, and despite much attention focused on the mechanisms of soot formation, many details of soot formation and oxidation still have not been understood [1]. In a diesel engine, soot can be produced as a result of high-temperature pyrolysis of the liquid fuel [2], and by accumulation of oxygen depleted fuel vapour [3]. Although the total oxygen content within the chamber of a diesel engine may be sufficient to produce an ignitable mixture, localised oxygen depleted regions often subsist. This is usually caused by insufficient mixing and results in soot being formed along with products such as hydrocarbons, carbon monoxide and hydrogen. By advancing the injection time, the fuel-air mixing can be significantly increased before combustion takes place and therefore the burning of the fuel becomes more complete. As a result, there are less oxygen-depleted zones and soot concentration is reduced. This enhanced mixing, however, leads to higher combustion chamber temperatures and pressures, which increase the nitrogen oxide content [4]. A number of attempts to reduce the emissions of nitrogen oxides from diesel engines exhaust were made. Albeit successful, most of them resulted in increased soot emissions [5-7].

Several attempts were made to obtain in-cylinder measurements of soot concentration within DI diesel engines. Most studies focused on the observation of soot location sites, evolution of soot concentration with time, and soot size distribution across the spray. Schraml *et al.* [8] observed that the initial rise in laser-induced incandescence (LII) signal coincided with the establishment of a diffusion flame. Soot formation was observed to initiate in the central region of the flame [9,10-13]. In this region, soot particle diameters are small and number density is high [10,14,15]. Soot particulates agglomerate as they travel down the plume and form larger particulates [10,12-14,16]. Soot is found throughout the combusting region, but at higher concentrations near the leading edge of the plume [9,17]. Studies by

Choi *et al.* [14] and Greis *et al.* [15], performed with swirl flows, have shown that the highest soot densities are found not near the leading edge of the plume but upstream, closer to the injector nozzle. They have also reported that higher soot temperatures are observed at the leading edge of the flames. Flynn *et al.* [12] observed that particulates were completely consumed by the hot diffusion flame sheath while high heat release rates persisted. The LII signal decay rate was found to be dependent on soot particles primary diameter [18]. Schraml *et al.* [18] also reported that cold start conditions did not alter soot size but increased soot concentration. It is believed that soot growth and oxidation were unaffected, but the initial number of soot particles significantly increased.

Only a few attempts were made to investigate the influence of engine parameters, such as injection pressure and timing, on soot parameters. It was found that for higher injection pressures (100 MPa compared to 50 MPa), soot was usually located further downstream of the spray [9,10,13], and the average soot volume fraction was reduced [10,13]. Bruneaux *et al.* [17] observed that for a 50% exhaust gas recirculation (EGR), significantly less soot was produced during combustion than without EGR. Exhaust particulates measurement made for the same conditions showed that, although EGR reduced soot formation during combustion, higher soot concentrations were emitted from the tailpipe. Bruneaux *et al.* [17] suggested that EGR significantly lowered the effectiveness of post-combustion soot oxidation.

2. Laser-Induced Incandescence

Laser-induced incandescence of soot particles was first observed in 1977 by Eckbreth when it interfered with coherent anti-Stokes Raman scattering measurements [19]. LII takes place when a laser beam hits particulate matter like soot. As the particles gain energy from the beam, their temperature increases and if the energy absorption rate is high enough, the soot particles will reach incandescent temperatures (4000 K) and produce near-blackbody emission. The radiation emitted has been shown to be nearly proportional to soot volume fractions [19-29]. As instantaneous planar measurements can be easily obtained, LII has emerged as an attractive and versatile technique for the measurement of soot concentrations in unsteady flows of complex geometry. For soot concentration measurements, LII has at least two significant benefits when opposed to other optical techniques, firstly it is fairly easily obtained through the use of a high-power laser, and secondly, its broadband radiation widens the range of collection strategies available to the experimenter. Subsequently, LII is widely used for investigations of in-cylinder soot formation [9,10,13,14,16,18,21,22], as well as for more general applications [23-33].

The light source usually preferred for LII is a frequency-doubled Nd:YAG laser running at 532 nm, with a pulse duration of about 7 ns at high power density (typically greater than 10 MW cm^{-2}). Even though a laser source at 266 nm would deliver a pulse of higher energy, and therefore ensure higher absorption efficiency, a source at 532 nm often proves to be a better choice since it offers the possibility to observe near-UV wavelengths, where little laser-induced emissions can be observed apart from LII. Hence the most widely reported use of LII was achieved with excitation at 532 nm and collection at wavelengths in the region of 400 nm. An ideal exposure time for LII imaging would be about 25 ns, in order to minimise interference from flame luminosity. A typical spectral filtering usually consists of a short-pass filter with cut-off wavelength at 400 to 450 nm and a 532 nm laser-line mirror to completely reject the strong elastic scattering of the laser. It is interesting to note that for widely used wavelengths (e.g. 400 nm) the collection signal is proportional to the mean soot diameter raised to the power of 3.4. It is therefore widely assumed that the LII signal is proportional to the soot volume fraction. A detailed theoretical analysis of LII is presented by Zhao and

Ladommatos [1], and a comprehensive study on the applicability of LII for soot measurements was performed by Wainner [34].

3. Experimental configuration

3.1 High-pressure diesel spray rig

The experiments were carried out using a rapid compression machine based around a Ricardo Proteus single cylinder engine converted to liner ported, 2 stroke cycle operation [35,36]. The removal of the valve train allowed the fitting of an optical chamber of 80 mm in height and 50 mm diameter into the cylinder head. The optical access to the combustion chamber was provided by four removable sapphire glass windows. Due to the increased volume of the combustion chamber the compression ratio was reduced to 9:1. To simulate a real diesel engine with a compression ratio of 19:1, the intake air was conditioned to give in-cylinder pressures and temperatures up to 12 MPa and 720 K, respectively. Prior to motoring the engine, the cylinder head was heated by a water jacket to 90°C and immersion heaters heated the oil to 75°C. The engine was motored by a dynamometer, via a 6:1 gearbox, to 500 rpm.

The fuel was delivered by a second generation Bosch common rail system. The high-pressure rail and the delivery pipe were both instrumented with pressure transducers. Fuel was supplied to the rail at pressures up to 160 MPa. The rail pressure, timing and duration of the injection were independently controlled by a custom-built fuel injection controller [35]. The injector was fitted with a single-hole valve-covered orifice (VCO) nozzle with a 0.2 mm diameter orifice. The nozzle had an equivalent cone angle of 130° and the injector was mounted at an angle of 25° to the horizontal in the cylinder head plate so that the spray propagated vertically into the optical chamber. The needle was of the single guided type and instrumented with a Hall effect needle lift sensor. The rising edge of the injection pulse was taken as a reference for the acquisition timing scheme and used to evaluate the cycle-to-cycle time variation of the image acquisition. The maximum variation was found to be within ±0.05 ms (i.e. ±0.15 CA).

The fuel used was a low sulphur reference fuel representative of automotive diesel with a density of 830 kg m^{-3} and sulphur content of 0.02% by mass. The addition of 0.04% of 2-ethylhexyl nitrate ($C_8H_{17}NO_3$) raised the cetane number from 55 to 57. The physical properties of the base fuel were not affected by the addition of 2-ethylhexyl nitrate although the timing of the various stages of combustion was changed [37]. 2-ethylhexyl nitrate was found to accelerate the early stage of autoignition, and had no significant effect on the combustion process after the ignition event.

The engine was kept at stable in-cylinder conditions for the duration of the recordings. These conditions are detailed in Table 1.

3.2 Laser-induced incandescence setup

The laser used was a pulsed Nd:YAG laser, capable of delivering pulses of 290 mJ at a frequency of 10 Hz and a wavelength of 532 nm. The laser pulses were spatially and temporally Gaussian with beam diameter of 8.7 mm and pulse width of 6-7 ns at full width at half maximum (FWHM). The laser mirrors and sheet-forming optics were optimised for high-reflectance of 532 nm wavelength and produced a laser sheet 55 mm high and 0.75 mm thick. The quoted pulse-to-pulse energy fluctuation was less than 3% and long term power drift less

than 5% over 8 hours. The laser system included an engine-synchronisation module that allowed the laser to run close to its optimum frequency (10 Hz) and still match the intrinsic frequency of the engine cycle. This was achieved by only making an acquisition when the operations of both the engine and the laser were synchronised, i.e. the engine was firing and the laser was ready to release a pulse. The Proteus operating speed was 500 rpm (i.e. 8.33 Hz) and was fired at a rate of 1:4 cycles (1 fired cycle followed by 3 non-fired cycles). Skipfiring was necessary to ensure proper purging of the combustion chamber and minimise window fouling by soot deposit. The firing frequency, approximately 2.08 Hz, is close to an integer fraction of the laser frequency (2.08×5 = 10.4 Hz). Considering that the allowed laser frequency range was from 9.30 to 10.90 Hz, a measurement could be performed for every fired cycle. The shift in laser frequency from 10.0 Hz to 10.4 Hz resulted in a 10% drop in pulse energy. Consequently the average pulse energy for the acquisition of the LII images presented in this paper was 255 mJ, corresponding to a power density of 88 MW cm^{-2} and a laser fluence of 0.6 J cm^{-2}.

The intensified CCD camera could acquire monochromatic images of up to 1280×1024 pixels with a frame rate of about 9 fps, and a 12 bit resolution. All LII images correspond to a field of view approximately 30 mm in width and 65 mm in height, with a resolution measured to be of 73×73 μm per pixel. An image-doubling extension was fitted onto the camera to duplicate the view of the combusting spray. Therefore, two views of the spray were recorded on one single image, and a different optical filtering could be applied to each half image. The original intention was to collect simultaneous LII and LIS of soot particles to produce maps of relative soot particle diameter. Although LII was successfully obtained with this configuration, LIS of soot could not be observed. Because the diesel droplets present during the injection scatter much more light than the soot particles, sufficient exposure of the soot scattering could not be obtained without the risk of overloading the photomultiplier tube with droplet scattering. An alternative would have been to gather simultaneous LII / LIS only after the injection had stopped, when no fuel droplets would be expected to be present. Unfortunately, it was observed that this constraint resulted in at least 50% of the soot formation period being discarded. It was also found that interference from LII was not negligible with the LIS filter, resulting in a potentially significant error. Therefore, it was decided that simultaneous LIS of fuel droplets would be recorded to complement the LII of soot. This strategy provides valuable information on the location of the liquid fuel spray relative to the soot formation regions. The main drawbacks inherent to this method lie in the necessity to set the image intensifier so that proper exposure is obtained for both LII and LIS, and the slight optical distortions caused by the optical arrangement. A schematic of the equipment layout used for simultaneous LII / LIS is shown in Fig. 1.

For LII imaging, a wide-bandpass filter was selected, with a measured peak transmission at 416 nm and FWHM of 64.4 nm. This filter maximised the LII signal and offered excellent rejection of interference from elastic scattering, fluorescence and flame luminosity. For LIS imaging, a narrow bandpass filter centred on the laser wavelength (i.e. 532 nm) was chosen with a 9.4 nm FWHM. A set of neutral density filters was used to avoid overloading the image intensifier and CCD camera. The image intensifier gate was open 5 ns before the laser pulse, and the total exposure was set to 40 ns. As the LII signal rise occurs approximately 10 ns after the start of the laser pulse [1], the LII signal was integrated for approximately 25 ns.

LII images were recorded throughout the soot formation period for three different injection pressures (100, 140 and 160 MPa) and a range of in-cylinder pressures (6, 7, 8 and 9 MPa at TDC for a non-fired cycle). Because of the turbulent nature of in-cylinder combustion, cycle-to-cycle variations in the position of dense soot regions were expected. This is accentuated by the fact that LII provides a map of soot concentration for a very narrow section of the flame. Therefore, although there may not be significant variations in the flame structure when

observed by high-speed video, the positions of dense soot regions may fluctuate greatly within the flame. Hence, consistent information on the characteristics of soot formation cannot be obtained without acquiring a range of images for every combination of engine parameters. Data sets were recorded from the start of soot formation until no soot could be detected, with a time interval between two sets of 0.33 ms (1 CA). Each data set included between 27 and 30 images acquired consecutively during the same run. All images were inspected visually to ensure they were recorded properly and that the repeatability was adequate. Data sets were then post-processed to produce ensemble averaged and standard deviation images for each condition. In order to simplify the presentation and analysis of the data, the mean intensity of each average image was calculated. The mean intensity provides a relative indication of the amount of soot recorded in each data set. The numbers thus obtained were used to produce the LII intensity profiles presented later. The influence of the data set size on the mean intensity was found to be small when more than 15 images were averaged. For data sets of at least 27 images, the coefficient of variation (ratio of standard deviation and mean intensity) was less than 1.7%.

3.3 Accuracy of the LII measurements

Tait and Greenhalgh [23] showed that for a Gaussian laser beam profile, the LII signal intensity is almost unaffected by variations in laser power density between 20 and 80 MW cm^{-2}. For this power density range, the error caused by laser fluence fluctuations has an average of 1.9% and a maximum of 3%. Since the laser system used for gathering the LII data had a power density between 60 and 90 MW cm^{-2}, it can be assumed that the results presented here were not significantly affected by shot-to-shot energy fluctuations and longer term fluence drifts. Another advantage lies in the fact that the progressive attenuation of the laser sheet across the dense soot regions of the spray will not result in a reduction of the LII signal. This significantly simplifies the post-processing and the interpretation of the LII data, since normalization of the images is not required.

Due to careful spectral and temporal filtering of the recorded radiation, no signals other than background noise were observed while the laser was momentarily switched off, suggesting that all signals recorded were laser-induced. The effects of flame luminosity on the LII data can therefore be deemed insignificant.

The vaporisation of soot particles induced by the laser results in the production of molecular carbon species (e.g. C_2, C_3). C_3, although believed to be the major vapour constituent, was not observed to produce emissions in LII studies [34]. C_2 is known to produce potentially intense emissions over a broad spectrum, especially at high laser intensities. Since some emission bands of C_2 (438.3, 473.7, 516.5 and 563.6 nm) are well within the preferred LII observation bandwidth, fluorescence from this molecule must be taken into account in order to ensure minimal (or at least quantified) contamination of the LII signal. Wainner [34] observed that for a laser fluence below 2 J cm^{-2} at 532 nm, the interference from C_2 fluorescence was not significant for collection wavelengths below 440 nm. The characteristics of the laser system used for this study satisfy this condition. Wainner [34] also reported that fluorescence from PAHs, although possibly significant at excitation wavelengths in the UV, was not detected for a laser wavelength of 532 nm. It is therefore concluded that the LII results presented here were not significantly contaminated by fluorescence from PAHs and C_2 molecules.

Ni *et al.* [26] showed that the LII signal intensity decay was highly dependent on soot particle diameter. They observed that the LII signal could first be detected between 10 and 12 ns after the start of the laser pulse and that the rise in signal intensity was unaffected by

particle size. Following the peak in LII signal intensity, a decay was observed to last up to several hundred nanoseconds. The decay time was shown to be longer for larger soot particles and Ni *et al.* thus recommended that LII signal should be imaged shortly after the laser pulse, with reduced exposure times so that size-dependence be minimised. The settings used for gathering the LII data presented here follow these recommendations, with an effective LII exposure time of 25 ns starting 10 ns after the start of laser pulse. It is estimated from Ni *et al.* [26] that the resulting error caused by size-dependence should be less than 4%.

Signal trapping, caused by regions of dense soot located between the laser plane and the CCD camera, is known to result in potentially considerable attenuation of the LII signal intensity. Estimation of the extent of signal trapping performed by Wainner [34] on laminar flames suggest that LII signals could be attenuated by as much as 45%. However, when used qualitatively, LII images still supply highly valuable information on timing and location of soot formation sites. Potentially, this technique can provide high-resolution data, both temporally and spatially, and has proven invaluable for improving the understanding of combustion processes in diesel engines.

It was observed that the time at which the LII images were recorded was accurate within 3%. The error caused by fluorescence, background noise and particle size dependence was estimated to be less than 6% for the LII data presented here. Since this value represents the proportion of spurious emissions within the LII images it can be concluded that it represents the overall measurement error, and consequently, 94% of the recorded intensities originated from incandescence of soot particles. Signal trapping by soot, window fouling and laser energy fluctuations can be seen as attenuations, rather than contaminations, of the LII intensity. Although their effects must be accounted for if quantitative data is required, they need not be accurately assessed for qualitative observations as long as they are not ignored altogether. In the present study laser energy fluctuations were found to affect the LII signal intensity by less than 3%, window fouling resulted in less than 20% attenuation, and LII signal trapping by soot was not quantified but was expected to be moderated by the use of the low-sooting fuel.

4. Results and discussion

4.1 Influence of in-cylinder pressure

Figures 2, 3 and 4 show LII intensity profiles for injection pressures of 100, 140 and 160 MPa, respectively, and a range of in-cylinder pressures. The effective nozzle opening durations are represented as solid black lines on the upper parts of each chart. They were obtained beforehand [38] with a high-speed video camera pointed at the nozzle orifice, with a frame rate of 27000 images per second. The uncertainty on the times of opening and closing of the orifice is 1 frame, corresponding to less than 0.04 ms (i.e. 0.12 CA).

It can be observed for all profiles that the time at which the LII signal was first detected appears to be independent of in-cylinder pressure.

For all conditions, LII profiles exhibit an almost linear increase in intensity before reaching a peak value. The actual amplitude of the peak, and the time at which the maximum intensity was reached, both appear to be unaffected by in-cylinder pressure. It can be observed from Figs. 2 to 4 that the LII signal intensity peaks are strongly related to the instant at which the nozzle closed. These observations appear to substantiate the speculations of Flynn *et al.* [12] that the end of production of soot precursors coincides with the end of injection. The swift LII signal intensity decay that follows is believed to correspond to the oxidation of the soot particles at the diffusion flame sheath. It can be concluded from the observation of Figs. 2 to

4, that changes in in-cylinder pressure did not markedly affected the amount of soot produced during combustion.

Examples of ensemble averaged images showing the influence of in-cylinder pressure on early soot formation are shown in Fig. 5. From these images it can be seen that for a 6 MPa in-cylinder pressure the average liquid fuel penetration length was 31 mm, and soot was found approximately 15 mm below the tip of the liquid spray. The initial soot formation regions spread over a height of 25 to 30 mm. It appears that the distance between the spray tip and the initial soot formation zone remained relatively constant at 15 mm for most conditions tested, although a slightly shorter distance (≈12 mm) was observed for some of the highest injection pressure cases.

While Fig. 5 provides information on the average location of soot and liquid fuel for a large number of cycles, individual LII images can give additional evidence on the structure of soot regions within the flame. In Fig. 6, instantaneous images obtained for early (2.2 ms ASOI) and late (3.9 ms ASOI) soot formation are presented. Simultaneous LIS measurement of liquid fuel is shown for the image recorded at 2.2 ms ASOI. As the injection ended at 3.6 ms, no liquid fuel was observed at 3.9 ms. The occurrence of fuel slugs and the clustered distribution of dense soot regions are apparent in Fig. 6. Although spray vaporisation and soot formation have been described as progressive and continuous processes [11,12], LII images of diesel sprays in the literature [9-11,13,15,17] clearly show clustered distributions similar to those presented here. It is expected that such detachments of groups of droplets should favour soot agglomeration and be strongly detrimental to soot oxidation because of the associated local depletion of oxygen. High frequency vertical oscillations (approximately 6.8 kHz) of the injector's needle were observed after the needle reached full lift. These pulsations are believed to impact on the delivery of fuel by the creation of slugs.

Examples of ensemble averaged images showing the influence of in-cylinder pressure on late soot formation are shown in Fig. 7. Unlike for the initial soot formation zones, soot regions at later times are unaffected by in-cylinder pressure. The location, dimension and intensity of the dense soot regions were not appreciably altered by changes in pressure from 6 to 9 MPa.

4.2 Influence of injection pressure

Figure 8 shows LII intensity profiles for an in-cylinder pressure of 6 MPa, and a range of injection pressures. Similar charts were produced for in-cylinder pressures of 7, 8 and 9 MPa. In all instances, the first appearance of LII signal seems to occur slightly earlier for the higher injection pressure cases (140 and 160 MPa). As discussed previously, a rise in LII signal intensity was observed for as long as the injection lasted. It is apparent from Fig. 8 that the rate at which the LII signal rises does not seem to be significantly affected by injection pressure. Since the maximum amount of soot that can be produced is directly related to the amount of injected fuel, and higher injection pressures result in higher injection rates, it is expected that an increase in injection pressure should be associated with an increased soot production rate. Although an increase in injection pressure from 100 to 160 MPa results in a 24% increase in injection rate, it is not clear whether a corresponding increase in soot production rate would be perceptible in Fig. 8. Following the rise in LII signal intensity, maximums are reached at the end of injections, with values that are dependent on fuel pressure. For all in-cylinder pressures tested, the highest injection pressures exhibited the lowest peaks in LII signal intensity.

Fig. 8 also shows the flame luminosity durations for an in-cylinder pressure of 6 MPa. As follows from this figure, higher injection pressures produced smaller quantities of soot. This

can be explained by the fact that higher injection pressures are generally believed to promote the production of smaller fuel droplets [39] which should, in turn, result in reduced local fuel vapour concentration, and ultimately to the formation of smaller soot particles that should be more rapidly oxidised. Higher injection pressures also result in longer spray penetration lengths and higher liquid core propagation velocities. Consequently, the transfer of momentum from the liquid spray to the gas phase should be enhanced, improving the mixing of the two phases. Since a better mixing quality corresponds to an increase in the local oxygen content, it is expected that oxidation of soot should be improved. The effects of momentum transfer are expected to be particularly important in the present study due to the quiescent nature of the in-cylinder charge prior to injection (i.e. non-swirl flow).

It can also be seen from Fig. 8 that flames lasted longer for lower injection pressures. This allowed more time for oxidation at the flame sheath. Since lower fuel pressures are known to result in higher particulate emissions [17], it can be concluded that the extended flame duration is not sufficient to oxidise the excess soot production.

An example of ensemble averaged images showing the influence of injection pressure on early soot formation is presented in Fig. 9, for an in-cylinder pressure of 8 MPa. Although the injection pressure has an apparent effect on liquid spray penetration length, the location of the first soot particles detected downstream of the tip of the spray remains almost constant. In Fig. 9 the distance from the nozzle to the first soot particles is about 37 mm, and an increase in fuel pressure from 100 MPa to 160 MPa induces a shift of less than 3 mm.

Fig. 10 illustrates the effect of fuel pressure on late soot concentration. While the lowest injection pressures appear to result in similar soot regions being formed, the LII image is noticeably different for an injection pressure of 160 MPa. The most striking difference is in the location of the soot region being approximately 10 mm closer to the nozzle orifice. This could be explained by the enhanced vaporisation observed for higher injection pressures (Bruneaux *et al.*, 1999), resulting in faster pyrolysis of the fuel. It is speculated that the formation of soot closer to the nozzle should be beneficial since interactions with the cylinder wall would be reduced.

It is also apparent from Fig. 10 that the LII signal has a more homogeneous and less intense appearance for the highest injection pressure, suggesting that the soot mass is better spread within the flame.

4.3 Detailed LII sequence

For the LII sequences presented thus far, the average time interval between two consecutive data sets was 0.33 ms (1 CA). It was observed that the original appearance of soot is a rapid process and therefore some details may not be apparent at such resolution. In order to obtain a finer series of LII images, the laser system software was automated to record a complete sequence with a data set interval of 50 μs (0.15 CA). The resulting sequence comprises 55 images, each image being itself the ensemble average of a 30-image data set. This sequence is presented in graphical form in Fig. 11, where each data point is the mean intensity of one ensemble-averaged image. The injection pressure was of 160 MPa, and the in-cylinder pressure and temperature were kept stable for the whole duration of the recording at 6 ± 0.2 MPa and 373 ± 6 K, respectively.

Comparing Fig. 11 with the previous LII profiles (Figs. 2 to 4), one can see that a finer temporal resolution produced a clearer representation of the phases of soot production. The LII signal intensity profile presented in Fig. 11 shows that three stages of soot production took place. The first stage is a rapid rise in LII signal that lasted for approximately 0.4 ms, corresponding to elevated soot production rates and low oxidation. The first detection of LII

signal was observed to occur at approximately the same time as the appearance of the flame luminosity. The diffusion flame, however, was established between 0.2 to 0.3 ms after the autoignition time as observed from autoignition high-speed video. This leads to establishment of the diffusion flame at a time between 2.3 and 2.4 ms in Fig. 11. Then the second stage in soot formation can be distinguished. At this stage higher soot oxidation rates and significantly more fluctuations in soot production are found. This slower soot production phase can be explained by the formation of soot from the ongoing injection, and the concurrent oxidation at the diffusion flame sheath. The third and final phase of soot formation is linked with the end of injection. It is recognised as a sudden decline in soot mass concentrations. While little soot is formed, the oxidation rates at the flame sheath are still high, resulting in a rapid fall in soot concentration.

5. Conclusions

By acquiring data sets of LII images throughout the soot formation periods for a range of elevated injection and fuel pressures, net soot mass production profiles were obtained for an extensive range of conditions. The conclusions drawn from the analysis of the simultaneous LII/LIS data are summarised below:

- Although high cycle-to-cycle variations in soot production were observed, the LII signal intensities were found to converge to a constant value when averaging of sufficient cycles was performed.
- The suggestion made by Flynn and co-workers [12] that the end of production of soot precursors coincides with the end of injection was corroborated by the results presented in this paper.
- From the analysis of the LII intensity profiles it appeared that the amount of soot produced during combustion was not noticeably affected by a change in in-cylinder pressure.
- Clustered distributions of soot were observed, similar to previously reported images although conflicting with the common approximation that soot is found evenly across the flame. It has been suggested that slugs of fuel detaching from the bulk of the liquid spray favoured soot agglomeration and inhibited soot oxidation due to the associated local depletion of oxygen. The formation of the slugs of fuel was linked to oscillations of the injector needle in the vertical direction. It is therefore suggested that a better mechanical control of the needle lift to reduce the vertical oscillations may result in a more continuous mixing between the liquid fuel and the ambient gas, ultimately leading to lower soot production.
- The combination of high-speed video recordings of flame and LII images of soot demonstrated a strong reduction in soot concentration across the diffusion flame sheath, confirming that oxidation rates at the flame sheath are high.
- The highest injection pressure (160 MPa) exhibited lower soot production and more homogeneous soot mass distribution within the flames, for all in-cylinder pressures cases. These effects have been related to smaller fuel droplets and better mixing quality, leading to smaller soot particles and improved oxidation, respectively.
- Although the diffusion flames produced with lower injection pressure lasted longer, it appeared that the extended oxidation time was not sufficient to oxidise the excess production of soot.
- Soot particles were detected closer to the liquid spray tip at higher injection pressures. This has been related to enhanced vaporisation of the liquid fuel. It is speculated that the

formation of soot closer to the nozzle should be beneficial since interactions with the cylinder wall would be reduced.

- The recording of a LII sequence at high temporal resolution has shown that three distinct phases in soot formation could be observed. High soot production rates were observed from the ignition time until the establishment of diffusion flame. Moderate soot formation rates were observed from the start of diffusion flame until the end of injection. High soot oxidation rates were seen from the end of injection.

Acknowledgements

The authors gratefully acknowledge the financial provision of the Nd:YAG laser system by the EPSRC (grant no. GR/R08094/01) and technical and financial support by Ricardo Consulting Engineers. The authors wish to thank John Evans (Case New Holland, Basildon, UK) for his assistance during the collection and analysis of the data, and Mike Monaghan for his valuable comments on this work.

References

1. Zhao, H., and Ladommatos, N., *Prog. Energy Comb. Science* 24:221-255 (1998).
2. Kennedy, I. M., *Prog. Energy Comb. Science* 23(2):95-132 (1997).
3. Bellan, J., *Reducing Soot in Diesel Exhaust*. NASA Tech Brief, 8(1), item 102, JPL Invention Report no. 5178/NPO-15715, 1984.
4. Brady, R. N. *Modern Diesel Technology*. Prentice Hall, New Jersey, USA, 1996.
5. Akagawa, H., Miyamoto, T., Harada, A., Sasaki, S., Shimazaki, N., Hashizume, T., and Tsujimura, K., SAE SP 1444, SAE, Warrendale, USA, 1999, pp. 19-32.
6. Christensen, M., and Johanson, B., SAE SP 1444, SAE, Warrendale, USA, 1999, pp. 11-19.
7. Shimazaki, N., Akagawa, H., and Tsujimura, K., SAE SP 1444, SAE, Warrendale, USA, 1999, pp. 1-10.
8. Schraml, S., Heimgärtner, C., Fettes, C., and Leipertz, A., Tenth Symposium (International) on Applications of Laser Techniques to Fluid Mechanics, Lisbon, Portugal, 2000.
9. Dec, J. E., Espey, C., Zur Loye, A. O., and Siebers, D. L., *Symposium on Mechanisms and Chemistry of Pollutant Formation and Control from Internal Combustion Engines*, The Division of Petroleum Chemistry, Washington, USA, 1992, pp. 1414-1429.
10. Kosaka, H., Nishigaki, T., and Kamimoto, T., SAE report no. 952451 (1995).
11. Dec, J. E., SAE SP 1244, SAE, Warrendale, USA, 1997, pp. 223-252.
12. Flynn, P. F., Durett, R. P., Hunter, G.L., zur Loye, A. O., Akinyemi, O. C., Dec, J. E., and Westbrook, C. K., SAE SP 1444, SAE, Warrendale, USA, 1999, pp. 117-132.
13. Inagaki, K., Takasu, S., and Nakakita, K., SAE SP 1444, SAE, Warrendale, USA, 1999, pp. 105-116.
14. Choi, D., Enami, M., Senda, J., Fujimoto, H., Kurata, K., and Asai, G., *Fifteenth Internal Combustion Engine Symposium (International)*, Seoul, Korea, 1999, pp. 315-320.
15. Greis, A. E., Grünefeld, G., Becker, M., and Pischinger, S., Eleventh Symposium (International) on Applications of Laser Techniques to Fluid Mechanics, Lisbon, Portugal, 2002.
16. Dec, J. E., SAE report no. 950456 (1995).
17. Bruneaux, G., Verhoeven, D., and Baritaud, T., SAE report no. 1999-01-3648 (1999).
18. Schraml, S., Will, S., and Leipertz, A., *Thirty-second Symposium (International) on Automotive Technology and Automation (ISATA)*, Vienna, Austria, 1999.
19. Eckbreth, A. C., *J. Appl. Phys.* 48(11):4473-4479 (1977).
20. Melton, L. A., *Appl. Optics* 23(13):2201-2208 (1984).
21. Dec, J. E., SAE report no. 910224 (1991).

22. Kock, B. F., Eckhardt, Th., and Roth, P., *Twenty-ninth Symposium (International) on Combustion*, Sapporo, Japan, 2002.
23. Tait, N. P., and Greenhalgh, D. A., *Berichte der Bunsengesellschaft fuer Physikalische Chemie* 97(12):1619-1625 (1993).
24. Filippov, A. V., Markus, M. W., and Roth, P., *J. Aerosol Sci.* 30(1):71-87 (1999).
25. Cignoli, F., Benecchi, S., and Zizak, G., *Appl. Optics* 33(24):5778-5782 (1994).
26. Ni, T., Pinson, J. A., Gupta, S., and Santoro, R. J., *Appl. Optics* 34(30):7083-7091 (1995).
27. Vander Wal, R. L., Jensen, K. A., and Choi, M. Y., *Combust. Flame* 109:399-414 (1997).
28. Vander Wal, R. L., *Combust. Flame* 112:607-616 (1998).
29. Roth, P., and Filippov, A. V., *J. Aerosol Sci.* 27(1):95-104 (1996).
30. Braun-Unkhoff, M., Chrysostomou, A., Frank, P., Gutheil, E., Lückerath, R., and Stricker, W., *Twenty-seventh Symposium (International) on Combustion, The Combustion Institute*, Boulder, USA, 1998.
31. Hilton, M., and Black, J. D., *Proceedings of SPIE*, The International Society for Optical Engineering, 1998, 3493:20-31.
32. Black, J. D., *Proceedings of SPIE*, The International Society for Optical Engineering, 1999, 3821:209-215.
33. Wainner, R. T., and Seitzman, J. M., American Institute of Aeronautics and Astronautics (AIAA) Journal 37(6):738-743 (1999).
34. Wainner, R. T., An Analytical and Quantitative Analysis of the Laser-Induced Incandescence of Soot. Thesis (PhD), Georgia Institute of Technology, USA, 1999.
35. Kennaird, D. A., Crua, C., Heikal, M., Morgan, R., Bar, F., and Sapsford, S., *Computational and Experimental Methods in Reciprocating Engines*, I.Mech.E. Conference transactions, Professional Engineering Publishing, London, UK, 2000, pp. 179-188.
36. Morgan, R., Wray, J., Kennaird, D. A., Crua, C., and Heikal, M., *2001 SAE Transactions – Journal of Engines* 110(3):389-399 (2001).
37. Higgins, B., Siebers, D., Mueller, C., Effects of 2-Ethylexhyl Nitrate on Diesel-Spray Processes, Report No. SAND98-8243, Sandia National Laboratories, 1998.
38. Kennaird, D. A., Crua, C., Lacoste, J., Heikal, M. R., Gold, M. R., and Jackson, N. S., *Diesel Engine Experiments*, SAE SP 1713, SAE, Warrendale, USA, 2002.
39. Di Giorgio, F., Laforgia, D., Damiani, V., *SAE International Congress and Exposition*, Detroit, USA, 27 February – 2 March 1995.

Tables

Table 1
Engine conditions for LII studies

Fuel	99.96% Esso AF1313 low sulphur +0.04% 2-ethylhexyl nitrate
Injected fuel quantity	30 mm^3
ICP for non-fired cycle	6, 7, 8, 9 MPa
Injection angle	-15 CA
Injection pressure	100, 140, 160 MPa
Intake temperature	373 K
Nozzle type	Single-hole VCO, 0.2 mm hole diameter

Figure captions

Fig. 1. Experimental set-up for LII study.

Fig. 2. LII signal intensity profiles for an injection pressure of 100 MPa and a range of in-cylinder pressures (6, 7, 8 and 9 MPa at non-fired TDC). Each data point represents the average intensity of at least 27 images. Times are relative to start of injection pulse (ASOI).

Fig. 3. As Fig. 2 but for an injection pressure of 140 MPa.

Fig. 4. As Fig. 2 but for an injection pressure of 160 MPa.

Fig. 5. Ensemble averaged images showing the influence of ICP on initial soot formation sites. Images were recorded between 2.0 and 2.2 ms ASOI, for an injection pressure of 160 MPa. ICPs were measured at non-fired TDC. Contrast was enhanced for clarity, white bars show ensemble averaged liquid fuel penetration obtained by simultaneous LIS, scales indicate distances from the nozzle in millimetres.

Fig. 6. Examples of liquid and soot clusters for early and late soot formation. 160 MPa injection pressure, 6.0 MPa ICP at TDC, times are relative to start of injection pulse. Contrast of images recorded at 2.2 ms showing simultaneous LIS (upper half) and LII (lower half) was enhanced for clarity. No LIS signal was observed at 3.9 ms.

Fig. 7. Ensemble averaged images showing the effect of ICP on late soot concentration zones. Images were recorded between 3.4 and 3.6 ms ASOI for an injection pressure of 160 MPa. ICPs were measured at non-fired TDC.

Fig. 8. LII signal intensity profiles for an in-cylinder pressure of 6 MPa at non-fired TDC and a range of injection pressures (100, 140 and 160 MPa). Each data point represents the average intensity of at least 27 images. Times are relative to the start of the injection pulse. The durations of the flame luminosity (obtained by still intensified CCD camera with 1 μs exposure) are indicated.

Fig. 9. Ensemble averaged images showing the effect of injection pressure on initial soot formation sites. Images were recorded between 2.0 and 2.3 ms ASOI, for an ICP of 8.0 MPa at non-fired TDC. Contrast was enhanced for clarity, white bars show ensemble averaged liquid fuel penetration measured by simultaneous LIS, scales indicate distances from the nozzle in millimetres.

Fig. 10. Ensemble averaged images showing the influence of injection pressure on late soot concentration zones. Images were recorded between 3.5 and 3.7 ms ASOI, for an ICP of 8.0 MPa at non-fired TDC. Scales indicate distances from the nozzle in millimetres.

Fig. 11. LII intensity profile for a 0.2 mm VCO nozzle with a 160 MPa injection pressure, 6 MPa in-cylinder pressure, and 720 K calculated temperature at TDC. Times are in milliseconds ASOI. Durations for injection pulse, nozzle opening and flame luminosity are indicated.

Figures

Figure 1

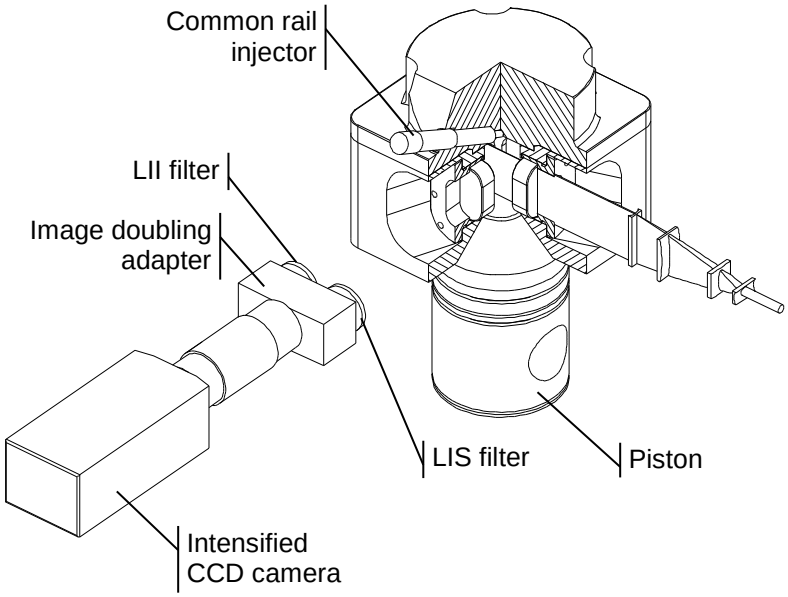

Figure 2

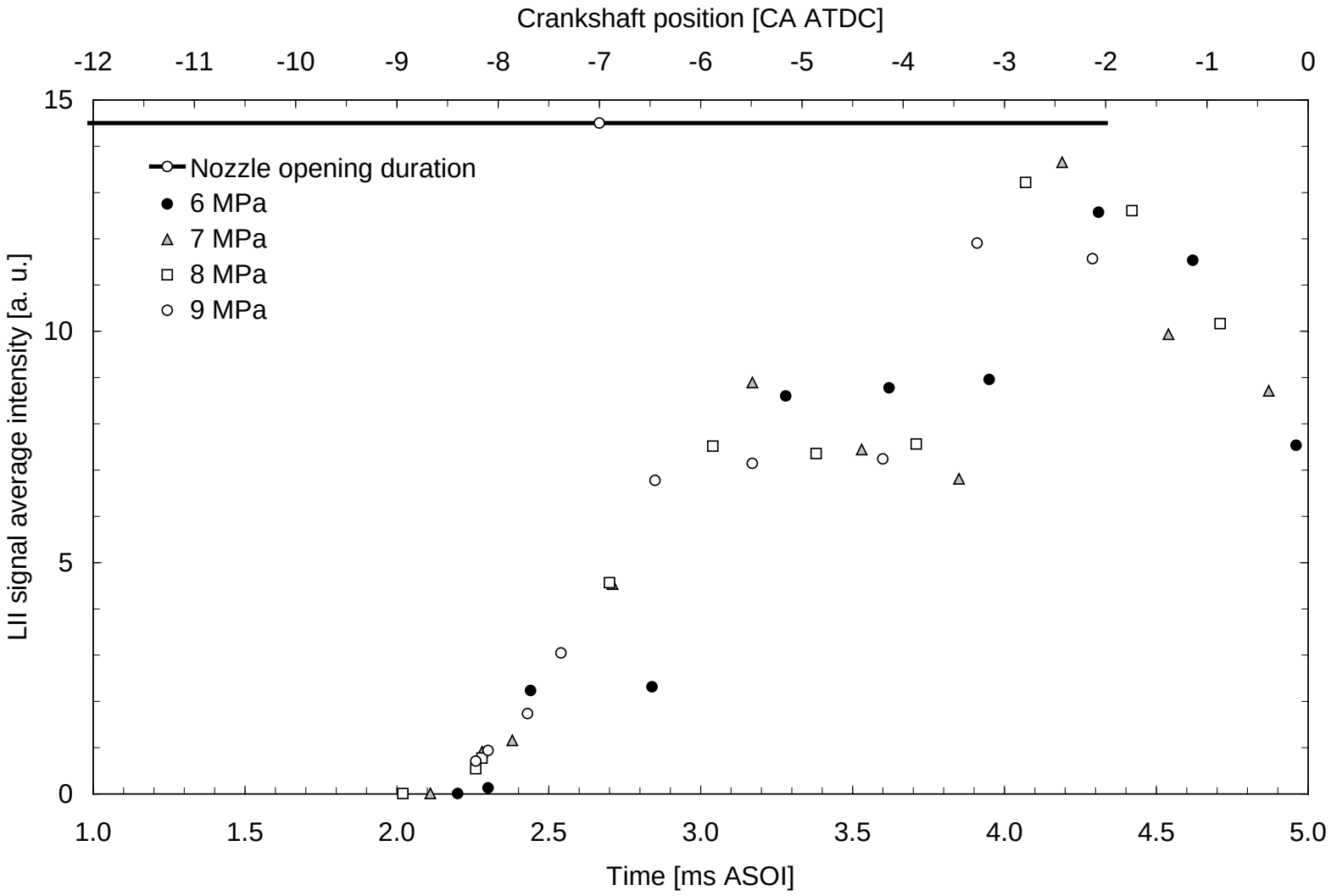
Crankshaft position [CA ATDC]
-12
-11
-10
-9
-8
-7
-6
-5
-4
-3
-2
-1
0
15
10
5
0
LII signal average intensity [a. u.]
Nozzle opening duration
6 MPa
7 MPa
8 MPa
9 MPa
1.0
1.5
2.0
2.5
3.0
3.5
4.0
4.5
5.0
Time [ms ASOI]

Figure 3

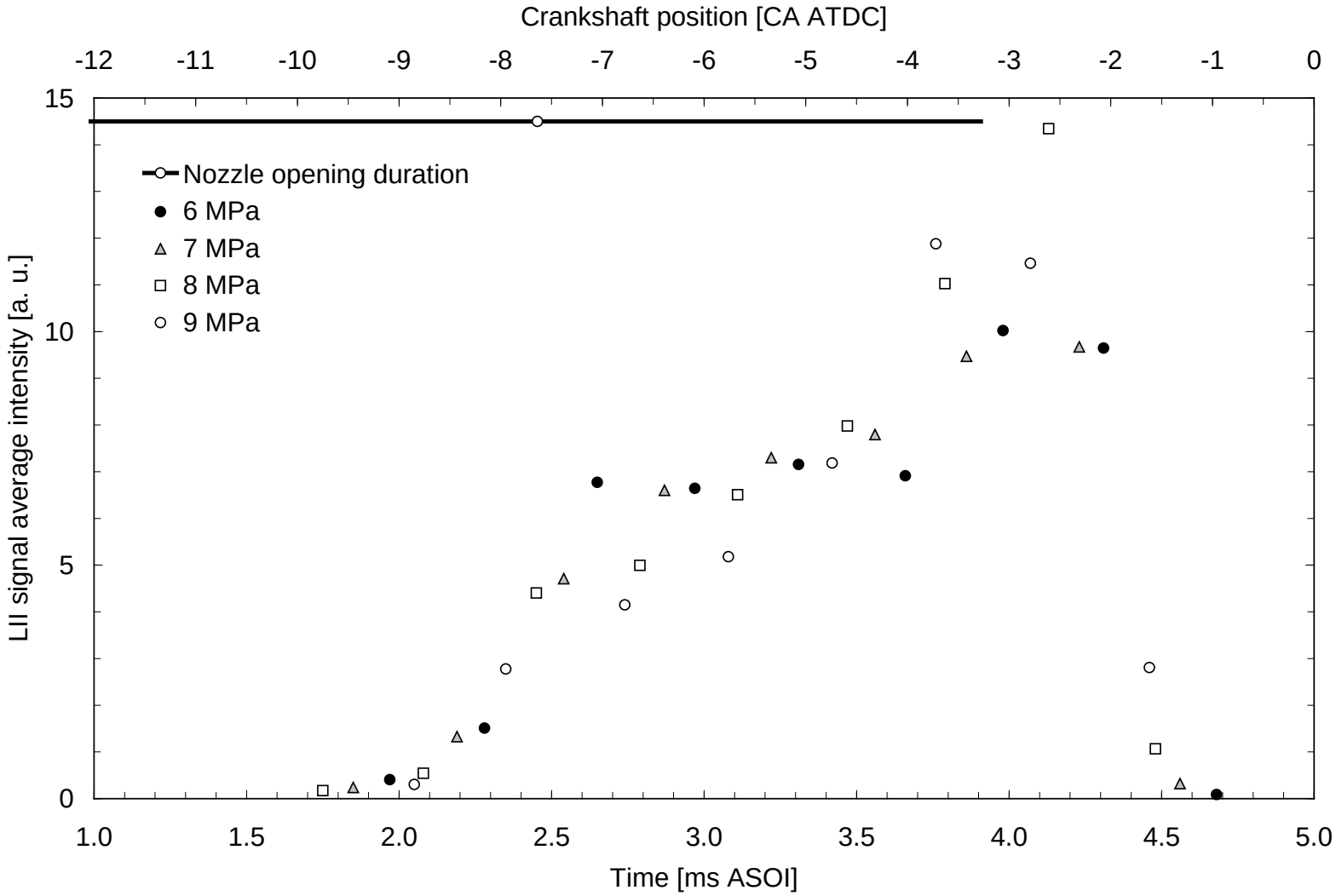
Crankshaft position [CA ATDC]
-12
-11
-10
-9
-8
-7
-6
-5
-4
-3
-2
-1
0
15
10
5
0
LII signal average intensity [a. u.]
Nozzle opening duration
6 MPa
7 MPa
8 MPa
9 MPa
1.0
1.5
2.0
2.5
3.0
3.5
4.0
4.5
5.0
Time [ms ASOI]

Figure 4

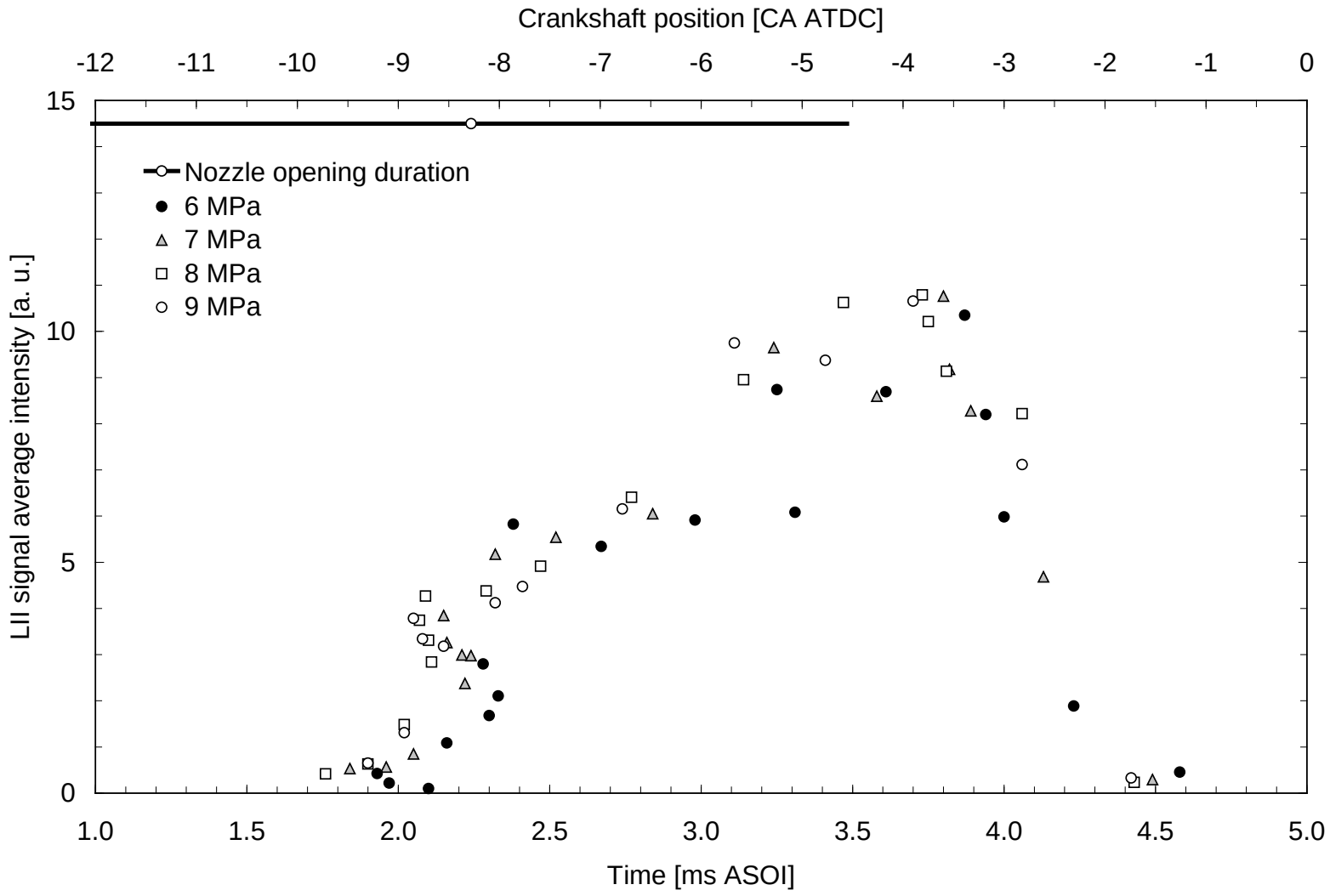
Crankshaft position [CA ATDC]
-12
-11
-10
-9
-8
-7
-6
-5
-4
-3
-2
-1
0
15
10
5
0
LII signal average intensity [a. u.]
Nozzle opening duration
6 MPa
7 MPa
8 MPa
9 MPa
1.0
1.5
2.0
2.5
3.0
3.5
4.0
4.5
5.0
Time [ms ASOI]

Figure 5

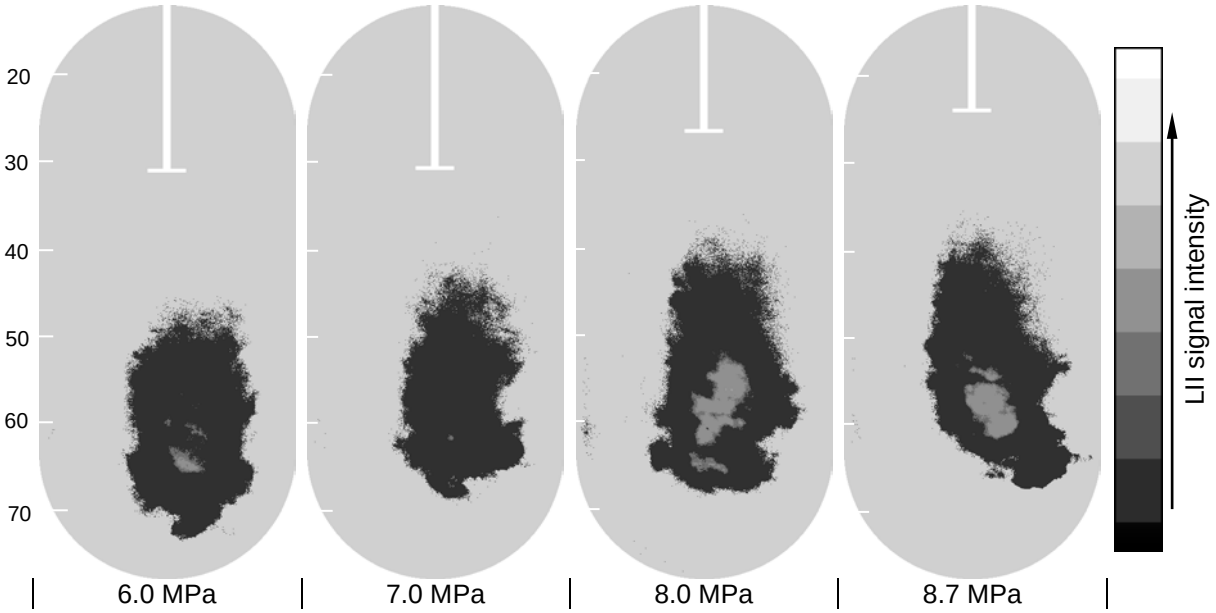

Figure 6

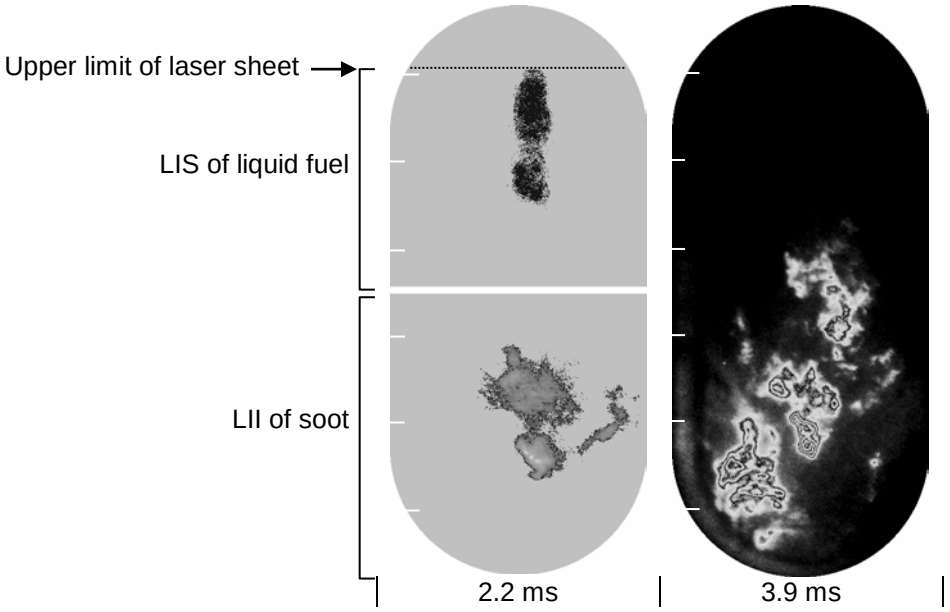

Figure 7

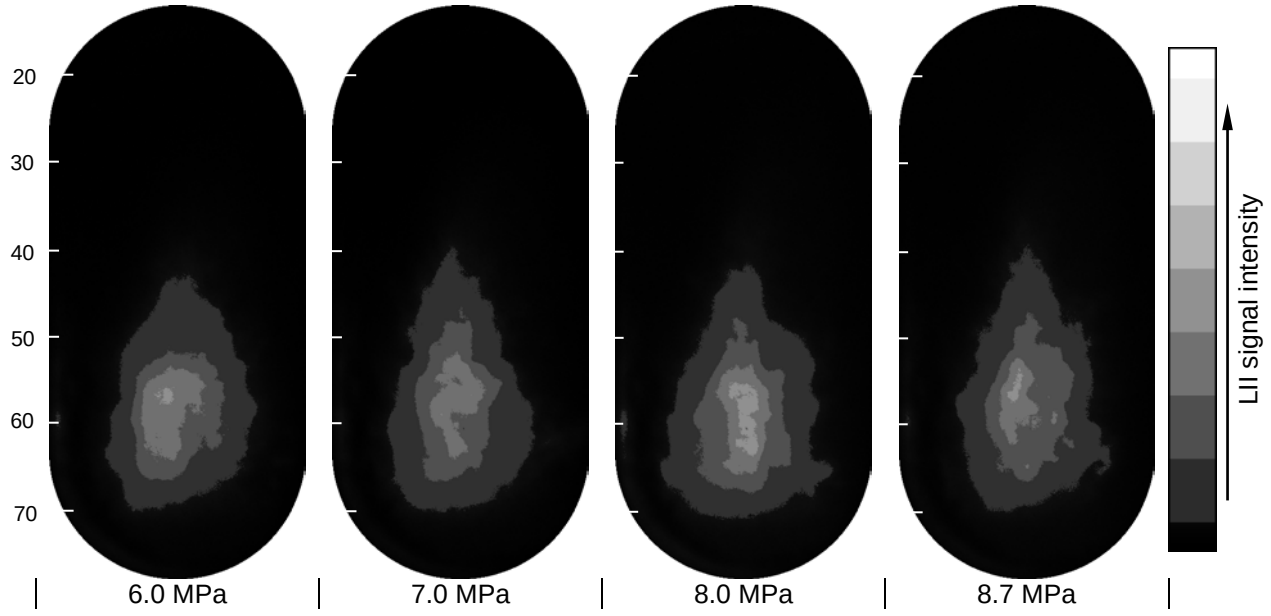
20
30
40
50
60
70
6.0 MPa
7.0 MPa
8.0 MPa
8.7 MPa
LII signal intensity

Figure 8

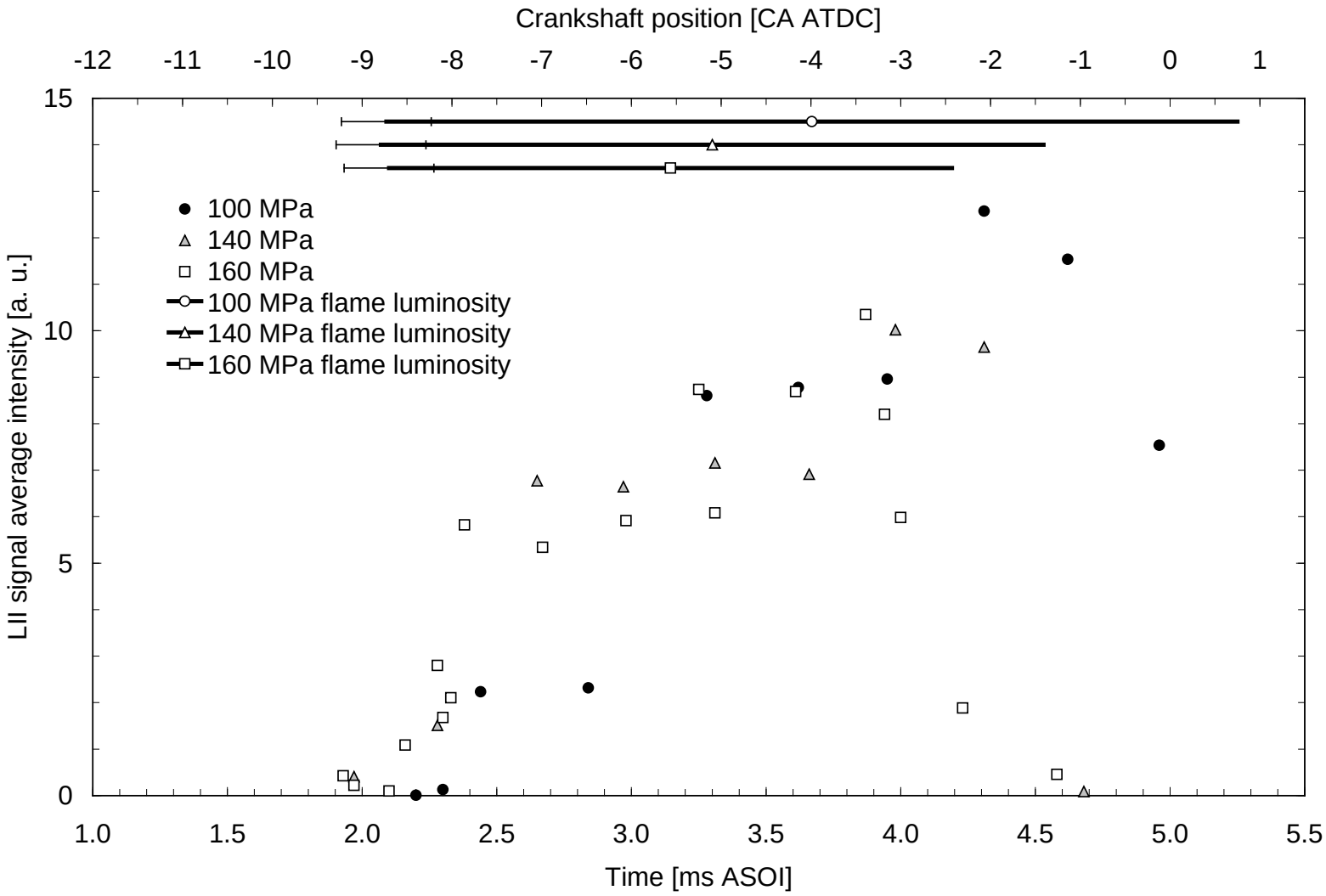
Crankshaft position [CA ATDC]
-12
-11
-10
-9
-8
-7
-6
-5
-4
-3
-2
-1
0
1
15
10
5
0
LII signal average intensity [a. u.]
100 MPa
140 MPa
160 MPa
100 MPa flame luminosity
140 MPa flame luminosity
160 MPa flame luminosity
1.0
1.5
2.0
2.5
3.0
3.5
4.0
4.5
5.0
5.5
Time [ms ASOI]

Figure 9

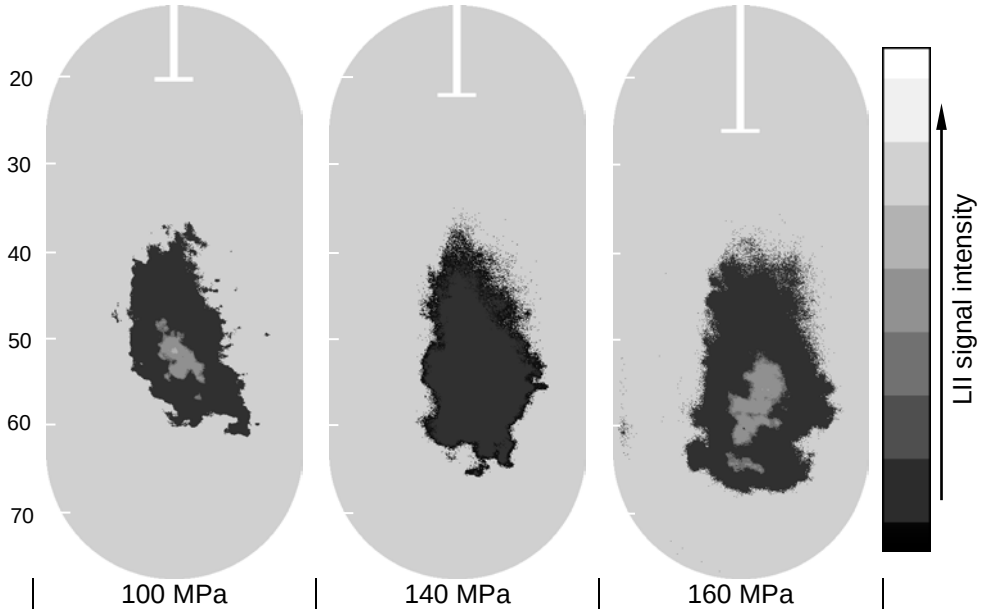

Figure 10

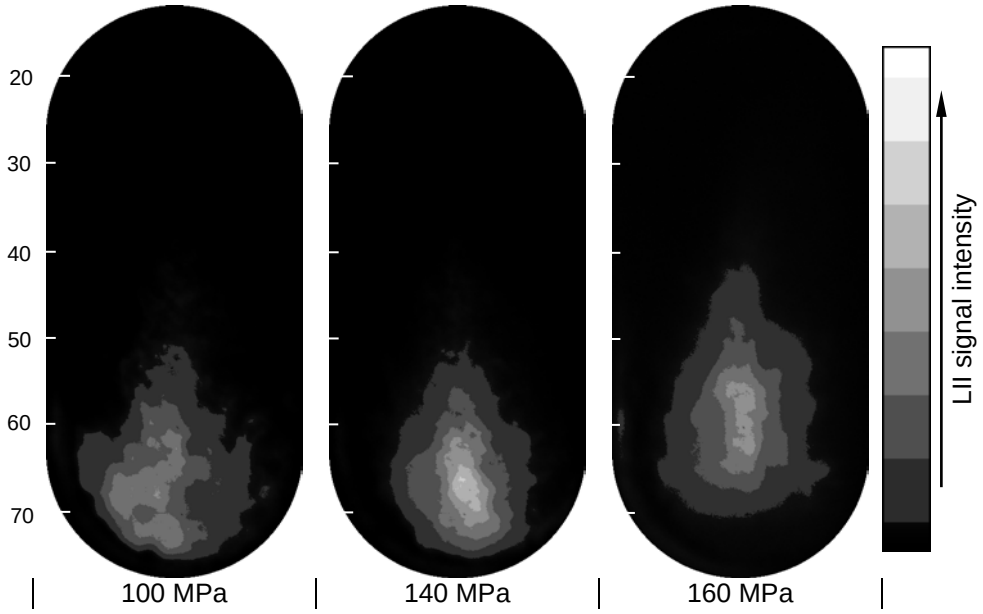

Figure 11

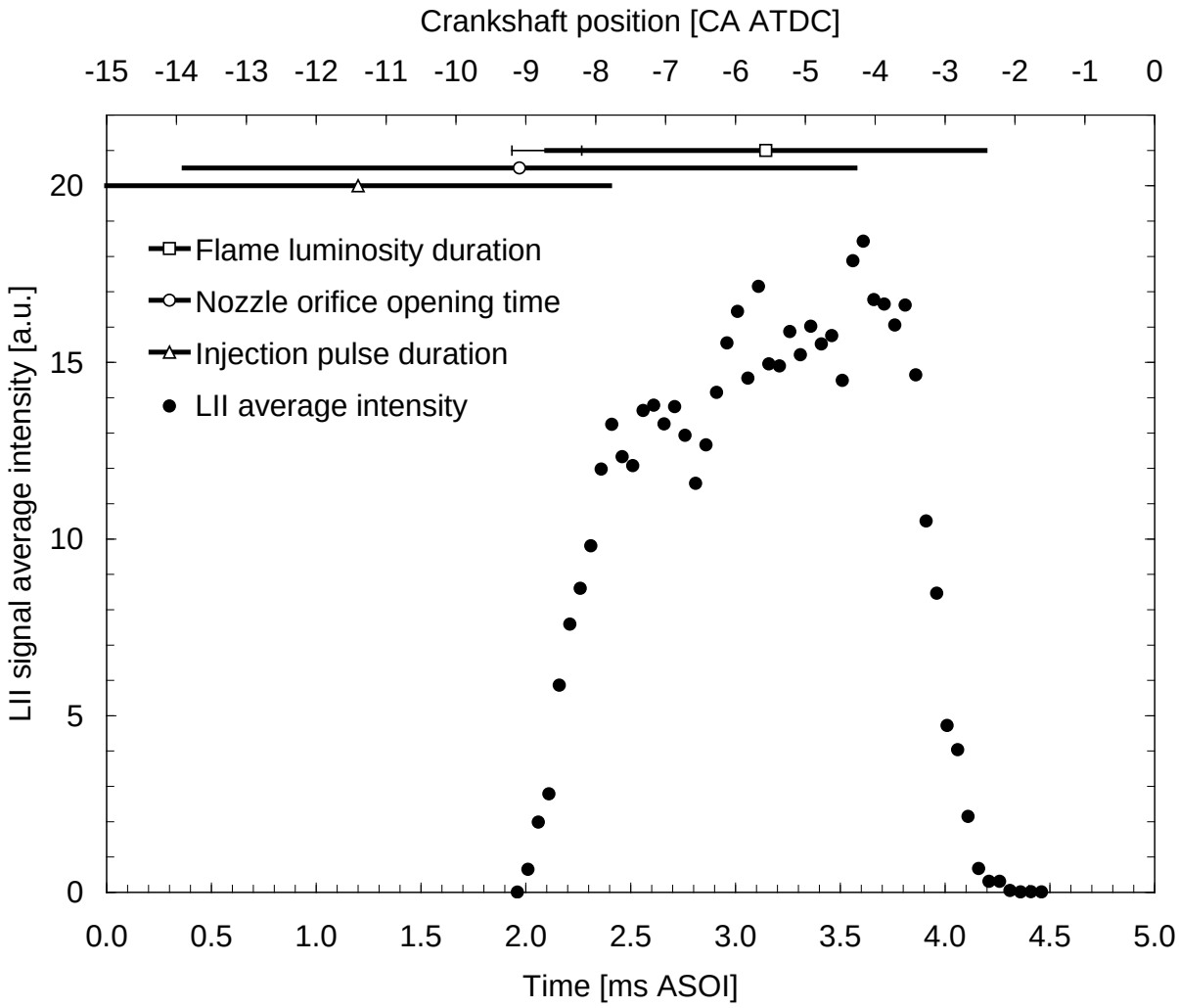
Crankshaft position [CA ATDC]
-15 -14 -13 -12 -11 -10 -9 -8 -7 -6 -5 -4 -3 -2 -1 0
Flame luminosity duration
Nozzle orifice opening time
Injection pulse duration
LII average intensity
LII signal average intensity [a.u.]
0 5 10 15 20
0.0 0.5 1.0 1.5 2.0 2.5 3.0 3.5 4.0 4.5 5.0
Time [ms ASOI]